



RESEARCH ARTICLE

Changes in snow water storage and hydrologic partitioning in an alpine catchment in the Colorado Front Range

Katherine E. Hale^{1,2,3} | Keith N. Musselman^{1,2} | Nels R. Bjarke^{4,5}  | Ben Livneh^{4,5} | Eve-Lyn S. Hinckley^{4,6}  | Noah P. Molotch^{1,2,7}

¹Department of Geography, University of Colorado at Boulder, Boulder, Colorado, USA

²Institute of Arctic and Alpine Research, University of Colorado at Boulder, Boulder, Colorado, USA

³Institute of Northern Engineering, University of Alaska Fairbanks, Fairbanks, Alaska, USA

⁴Cooperative Institute for Research in Environmental Science, University of Colorado, Boulder, Colorado, USA

⁵Department of Civil, Environmental, and Architectural Engineering, University of Colorado, Boulder, Colorado, USA

⁶Department of Ecology and Evolutionary Biology, University of Colorado, Boulder, Colorado, USA

⁷Jet Propulsion Laboratory, California Institute of Technology, Pasadena, California, USA

Correspondence

Katherine E. Hale, Department of Geography, University of Colorado at Boulder, Boulder, CO, USA.
Email: kehale3@alaska.edu

Abstract

As the climate warms, snow-dominated regions are increasingly susceptible to precipitation phase changes and earlier snowmelt. In alpine catchments, snowmelt is the majority of runoff, governed by heterogeneous interactions among snowfall, wind, topography and vegetation. The role of the alpine snowpack in delaying the downstream release of accumulated snowfall remains understudied, despite its fundamental role in sustaining lower-elevation ecosystems and populations. We evaluated fine-scale changes in the magnitude and duration of alpine snow water storage and release by comparing effective precipitation seasonality to that of surface water inputs using a Snow Storage Index (SSI). We forced the Distributed Hydrology Soil Vegetation Model with historical climate conditions and an end-of-century warming signal down-scaled from a 4-km regional climate model, to simulate future changes in snow water storage and partitioning of precipitation to runoff and evapotranspiration. The hydrological modelling was conducted on a 2-m spatial grid to resolve fine scale processes over a 0.6-km² headwater catchment within the Niwot Ridge Long-Term Ecological Research site located in the Rocky Mountains, Colorado, USA. Proportionally more rainfall, reduced snowpack size and extent, and earlier snowmelt occurred in the future scenario with decreased catchment average SSI and thus snow water storing capabilities, with inordinately large decreases occurring in areas of the catchment with reconstructed snowdrifts (–57% average and –100% maximum). Using the Budyko framework to evaluate annual hydrologic partitioning, precipitation inputs to streamflow increased by a maximum 10% in large SSI regions with snowdrifts under warming conditions, signifying a potential buffer for total catchment and annual streamflow loss in a future climate. The fine-scale analysis of hydrologic sensitivities to warming presented herein are important because climate conditions are expected to further reduce alpine snow water storage, alter hydrologic partitioning, and runoff generation for ecosystems and people living downstream.

KEYWORDS

alpine catchment, Budyko, climate change, DHSVM, hydrologic modelling, hydrologic partitioning, snow water storage, surface hydrology

1 | INTRODUCTION

Seasonal snowpack is an essential component of Earth's hydrological cycle. About one-sixth of the global population relies on seasonal snowpack and glacier-derived runoff as a primary water resource (Barnett et al., 2005; Pörtner et al., 2019). Snowmelt contributes to regional water supply and partially dictates the timing and amount of downstream water resources, as it is released from the snowpack days to months after snowfall (Immerzeel et al., 2020; Mote et al., 2018; Viviroli et al., 2007). The magnitude and duration of regional water storage in the snowpack is thus a function of precipitation phase—rainfall or snowfall—and the subsequent timing of water release as snowmelt, which are primary mechanisms controlling the amount of downstream water availability and are highly sensitive to climate change (Berghuijs et al., 2014; Foster et al., 2016). The timing of water release from the snowpack is, in turn, influenced by regional climatic conditions and orographic enhancement of snowfall (e.g., sustained winter temperatures and wind redistribution), which vary significantly across the globe (Mott et al., 2018).

Alpine regions often represent a small percentage of headwater catchment area yet generate a disproportionate amount of the total catchment discharge (Knowles et al., 2015). Runoff from alpine catchments during the snowmelt period can account for more than 80% of total annual runoff (Campbell et al., 1995; Kattelmann & Elder, 1991), serving as an important water resource for human consumption, agriculture and industry (Clow et al., 2003). However, spatially, the snowpack distribution across these regions is often extremely heterogeneous (Blöschl et al., 1991; Blöschl & Kirnbauer, 1992; Freudiger et al., 2017), due to strong winds and variable interactions among snowfall accumulation, vegetation and topography (Jenicek et al., 2018; Winstral et al., 2013). Thus, high-resolution analyses of snow water storage are needed in alpine systems for improved understanding of the environmental processes controlling water availability and runoff generation (Clow et al., 2003; Griessinger et al., 2019; López-Moreno et al., 2011, 2013; Winstral & Marks, 2002).

The spatial variability of the snowpack in alpine watersheds has been thoroughly explored (e.g., Badger et al., 2021; Bilish et al., 2019; Brandt et al., 2020; Mazzotti et al., 2019; Vionnet et al., 2019), as have the effects of snowpack variability on intra-basin snowmelt heterogeneity (Marks & Winstral, 2001), basin ecology (Baron & Denning, 1993; Hermes et al., 2020) and water chemistry and hillslope erosion (Tarboton et al., 1991). Yet, how variability in the snowpack, particularly snow water equivalent (SWE), drives spatial variability in snow water storage and runoff generation remains understudied, particularly at the fine resolution (<100 m) required to capture extreme heterogeneity in small, topographically complex alpine catchments. Specifically, the spatially distributed relationship between snow water storage, defined here as the difference in magnitude and timing between precipitation and surface water inputs (SWI) available to the terrestrial system (rainfall or snowmelt), and the surrounding and downstream hydrology has yet to be evaluated in these regions.

Climate warming has caused fundamental hydrologic changes in mountainous regions of the western United States, with variable

effects on the sensitivities of water availability (Berghuijs et al., 2014; Foster et al., 2016; Hale, Jennings et al., 2023; Hinkley et al., 2012; Livneh & Badger, 2020). In the last century, there has been a gradual precipitation phase shift from snowfall to rainfall, decreases in peak SWE accumulation, earlier onset of snowmelt and shorter snow cover duration in mountainous regions across the United States and globally (Hammond et al., 2018; Mote et al., 2018; Musselman et al., 2021). In response, several previous climate warming studies have reported catchment average net decreases in annual runoff and net increases in annual potential evapotranspiration (PET) (Anghileri et al., 2016; Clow, 2010; Liu et al., 2022; Mahanama et al., 2012; Tang & Lettenmaier, 2012).

Snowfall redistribution by wind directly impacts the spatial heterogeneity in effective precipitation—that which remains in a given area after wind redistribution causes drifting of snow (Badger et al., 2021; Winstral & Marks, 2002). Simulated climate warming has been shown to influence maximum SWE, interannual hydrologic variability and water and energy limitations disproportionately across a single catchment, with the greatest snowpack decreases and water limitations occurring in snowdrifted regions (Marshall et al., 2019). Thus, the reduced annual snowfall fraction (amount of annual precipitation falling as snow), altered snowfall redistribution, and earlier snowmelt timing directly affect the amount and timing of snow water storage and the associated variability across an area, particularly those regions storing more water in the snowpack for longer durations. Heterogeneous snowpacks across alpine regions, which are highly susceptible to wind redistribution of snowfall, have cascading consequences for the amount and timing of regional water availability and delivery to lower ecosystems and human communities (Barnhart et al., 2016; Harpold et al., 2012; Marshall et al., 2019; Trujillo et al., 2012; Trujillo & Molotch, 2014).

Historically, a singular spring–summer snowmelt pulse has, with relative efficiency, overwhelmed soil moisture deficits and soil field capacity and increased overall hydrologic partitioning to runoff (Barnhart et al., 2016; Hale, Musselman, et al., 2023; Liu et al., 2022). Future reductions in the magnitude of this seasonal snowmelt pulse may reduce annual hydrologic partitioning to runoff since soils will be less saturated throughout spring and early summer months (Liu et al., 2022). However, a warming-induced shift towards earlier rainfall and snowmelt events will also misalign the timing of catchment water availability (i.e., rainfall or snowmelt) and evaporative demand (i.e., PET) and increase cold-season—and potentially annual—hydrologic partitioning to runoff (Foster et al., 2016; Hale et al., 2022; Liu et al., 2022). It is unclear how future warming-induced changes in snow water storage may alter partitioning of SWI (rainfall or snowmelt) to runoff. Yet, it is expected that variability in PET and runoff will exist across a single alpine catchment now and in the future, given the high spatial variability of effective precipitation (Clow, 2010; Harpold et al., 2012; Knowles et al., 2006; Pörtner et al., 2019).

In this study, we sought to quantify the consequences of climate warming on snow water storage and associated hydrologic partitioning across an alpine catchment. We ask *how does the spatial distribution of snow water storage influence hydrologic partitioning in an alpine*

catchment? and how will future changes in climate influence snow water storage and hydrologic partitioning? By modelling historical and future climate conditions in a snow-impacted, headwater catchment, we evaluated the hypotheses that an increase in the temporal misalignment of water availability and PET, by way of earlier rainfall and snowmelt with warming air temperatures, will either increase or decrease relative downstream catchment runoff magnitude (Hale, Musselman, et al., 2023; Kormos et al., 2014; Foster et al., 2016).

2 | STUDY AREA

This study was conducted in a 0.6-km² alpine headwater catchment within the Niwot Ridge Long Term Ecological Research (NWT LTER) site, located in the Front Range of the Colorado Rocky Mountains, 40-km northwest of Boulder, Colorado, USA (Figure 1a) (Bjarke et al., 2021; Bowman & Seastedt, 2001). The entire NWT LTER site spans from the Continental Divide downward in elevation to the sub-alpine forest. The Saddle Catchment (Figure 1a) is an alpine basin with an average elevation of 3528-m a.s.l. and is located 5.6-km east of the Continental Divide, receiving the large majority (~80%) of its approximately 1035 mm catchment-average annual precipitation as snowfall (Bowman & Seastedt, 2001; Caine, 1995; Greenland, 1989; Jennings & Molotch, 2019). Average daily temperatures of -7.6°C in autumn months, -12.3°C in winter months, -4.1°C in spring months and -0.5°C in summer months (Bjarke et al., 2021; Jennings & Molotch, 2019) support a persistent snowpack within the small, headwater catchment throughout the year and a short growing season for alpine vegetation (1–3 months) (Jones, 2001). As such, the catchment experiences significant snowmelt generation and subsequent runoff in mid-to-late spring season each year (Bjarke et al., 2021).

Five land cover types are predominant across the Saddle Catchment: bare ground, alpine meadow, open shrub, closed shrub and evergreen broadleaf forest (Figure 1b). These land cover types were

defined by the National Ecological Observatory Network (NEON) biomass dataset (Neiman et al., 2011). Windswept, bare ground exists primarily in the northwest corner and in the central region of the catchment. Alpine dry meadow covers the largest extent of the catchment (~55%) and exists along the perimeters of open and closed canopy shrubs, which also grow in the central regions of the catchment (Hermes et al., 2020). The evergreen broadleaf forest exists in the southern, lower-elevation portion of the catchment (Figure 1b). Land cover types differ in overstory and understory density, and thus significantly influence the amount of water that is evapotranspired versus is eventually partitioned as catchment runoff. Photographs of the predominant Saddle Catchment land cover are available in Hermes et al. (2020).

The study catchment experiences significant wind exposure (Jepson et al., 2012), often resulting in significant redistribution of snowfall during autumn, winter and spring months. Prevailing winds are from the west (Barry, 1973; Winstral et al., 2002). Wind deposition, snowdrifted regions typically exist in the northwest and central portions of the catchment, which receive most redistributed snowfall, likely producing more SWI and runoff due to an almost year-round persistent snowpack (Bowman, 1992). A wind-scoured area persists on the eastern portion of the catchment; often it is water-limited (Bowman, 1992).

3 | METHODS

To evaluate the influence of climate warming on snow water storage and associated hydrologic partitioning across the Saddle Catchment, we first used a previously developed index of snow water storage (hereafter the Snow Storage Index [SSI]) (Hale, Jennings, et al., 2023). The SSI across the Saddle Catchment was derived by quantifying the difference in magnitude and timing of annual precipitation and the magnitude and timing of annual SWI (rainfall and snowmelt) (Hale,

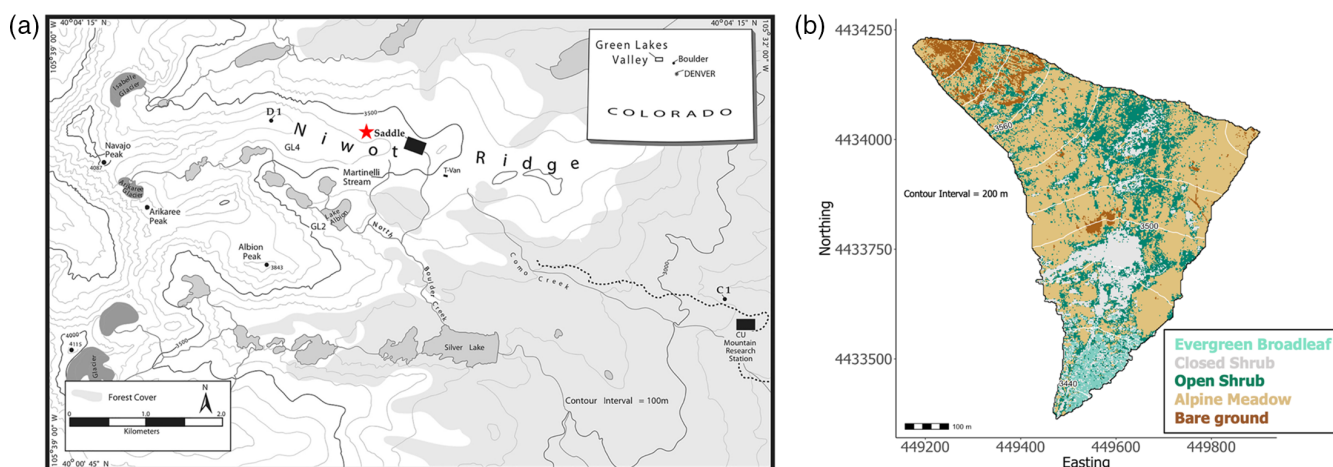


FIGURE 1 (a) Niwot Ridge Long Term Ecological Research spanning alpine to sub-alpine terrain, the Saddle Catchment labelled with a red star (modified from Rush and Rajaram, 2022), (b) Saddle Catchment coloured by land cover types, guided by the NEON biomass data (NEON, 2020): bare ground, alpine meadow, open shrub, closed shrub and evergreen broadleaf forest.

Jennings, et al., 2023), which were spatially represented historically and into the future using a hydrologic model, supported by meteorological and streamflow observations. The use of the SSI affords an explicit comparison of the amount and duration of water that is stored in the regional snowpack, which we compared to modelled annual partitioning of water inputs to evapotranspiration (ET) and runoff (Q) using the Budyko framework (Budyko, 1974). To evaluate the influence of snow water storage on hydrologic partitioning, we regressed long-term proportional runoff estimates against the SSI and a sub-annual ratio of its components. A full description of each methodological step in this analysis follows.

3.1 | Hydrologic modelling

We used the Distributed Hydrology Soil Vegetation Model (DHSVM) (Wigmosta et al., 1994) to evaluate alpine snow water storage and hydrologic partitioning for this study. Recently, DHSVM has been developed to accurately simulate hydrology in mountainous catchments (Badger et al., 2021; Currier et al., 2022; Hale et al., 2022; Sun et al., 2019). The model uses a dynamic lateral routing scheme, which is intended to capture runoff dynamics in these landscapes (Brooks et al., 2004; Livneh et al., 2014, 2015; Whitaker et al., 2003). DHSVM's snow model resolves a two-layer energy balance model for snow accumulation and snowmelt (Raleigh et al., 2016; Wigmosta et al., 1994). Soil moisture and surface runoff are computed via a multi-layer unsaturated soil model and a saturated subsurface flow model. Evapotranspiration (both ET and PET) is computed using a Penman-Monteith approach via a two-layer canopy representation. The model considers the influences of terrain slope and aspect on incoming shortwave and longwave radiation within the surface energy budget. DHSVM can additionally be provided with dynamic observations for solar shading as well as a gridded estimate of the mean diurnal cycle of cloud-free incoming solar radiation each month. We ran DHSVM at a 2-meter spatial resolution on an hourly timestep.

With respect to modelling streamflow, DHSVM simulates the exchange of water between grid cells, resulting in a three-dimensional redistribution of surface and subsurface water across the landscape (Wigmosta et al., 1994). It moves water between grid cells as overland flow, channel flow and/or shallow subsurface flow in the soil. The subsurface water storage in the soil is a function of soil depth and depth to the root zones in each soil layer, where increased soil depth allows for increased storage (McNamara et al., 2005). The soil-vegetation water balance accounts for rooting zone water storage, overstory and understory interception, evaporation and transpiration, surface soil evaporation, snowpack water content and precipitation (Wigmosta et al., 1994). Impermeable bedrock underlies the defined water table (Wigmosta et al., 1994). All non-intercepted rainfall or snowmelt enters the soil column and becomes subsurface storage. Once the soil becomes saturated, excess water becomes surface runoff (Wigmosta et al., 1994).

For our study, the majority of DHSVM soil, land cover and snow parameters were obtained from previous applications of DHSVM over the Boulder Creek Watershed (Badger et al., 2021; Livneh et al., 2014, 2015), since our study catchment is at the headwaters of this larger basin and these past simulations yielded realistic snowmelt and runoff dynamics. Thus, the model configuration outlined in Livneh et al. (2014, 2015) was used here to provide initial settings for soil and vegetation parameters, and spatial distribution of land cover was updated using the NEON biomass data (Figure 1b) (Neiman et al., 2011). Additional parameter adjustments were made following a calibration scheme intended to effectively reproduce the annual cycle (r^2) and total volume (percent bias) of observed runoff (Bjarke et al., 2022). In order to account for uncertainty in the estimation of soil and snow parameters, a range of values ranging between factors of $0.25\times$ and $4\times$ the original values in Livneh et al. (2014, 2015) were selected for the calibration process based on both observations made within the Niwot LTER (Hermes et al., 2020) and previous DHSVM simulations made within the region (Badger et al., 2021). We applied a Latin hypercube sampling technique (Stein, 1987) to select 100 sets of potential parameter configurations and selected the final set of parameters that produced a simulation optimizing both r^2 and percent bias when compared to the observed runoff over the study period (Bjarke et al., 2022). We subsequently analysed DHSVM output in a stratified manner based on the five predominant land cover types within the catchment.

3.2 | Historical scenario

Historical snow water storage and hydrologic partitioning were assessed using DHSVM outputs from 1 October 2000 to 30 September 2019. This model simulation ran with hourly forcing data measured at one meteorological station within our study catchment, which were spatially distributed based on model sub-routines (Bjarke et al., 2021; Jennings et al., 2021). Precipitation falling as snow was redistributed in DHSVM using a SWE reconstruction model to obtain accurate spatially distributed patterns of SWE across the catchment (Jepsen et al., 2012). The SWE reconstruction model output was used to derive monthly spatial weights to represent effective precipitation across the catchment and thus the vast heterogeneity of the alpine snowpack due to wind-blown snowfall (Badger et al., 2021; Jepsen et al., 2012). SWE reconstructions are only valid from peak SWE through the melt season. Thus, during fall, winter and early spring accumulation months, snowfall was distributed based on the weights generated during the melt season, from peak SWE onward (for more information, see Badger et al., 2021; Jepsen et al., 2012). Precipitation falling as rain was uniformly distributed across the domain. Gauged stream discharge observations at the outlet of the study catchment were used for model calibration and validation (Caine et al., 2023). A dense array of sensor nodes collects soil moisture and temperature information and was used to validate the land cover layer; and underlying geology of the catchment was downscaled using a nearest

TABLE 1 Data sources and associated record lengths and spatial and temporal resolutions used in the historical and future DHSVM scenarios.

Variable	Units	Record length	Resolution	Reference
Meteorological forcings	Precipitation (mm), temperature (°C), wind speed (m/s), relative humidity (%), solar radiation (W/m ²)	1990–2019	Hourly, point	Jennings et al., 2021
Effective precipitation weights	No units	1996–2007	Monthly, 30-m	Jepsen et al., 2012
Streamflow	l/s	1999–present	Daily, point	Caine et al., 2023
Soil moisture and temperature	% and °C	2018–present	10-minute, point	Methodology outlined in Kerkez et al., 2012
Underlying geology type	No units	2017	Long-term, 30-m	Horton, 2017
End-of-current-century delta values	Temperature (°C), relative humidity (%), and longwave radiation (W/m ²)	2000–2013	Daily, 4-km	Liu et al., 2017

neighbour algorithm. All mentioned datasets used in this study are listed and further described in Table 1.

3.3 | Future scenario

To emulate representative concentration pathways (RCP) 8.5 projected 2071–2100 climate warming, the Weather Research and Forecasting (WRF) pseudo global warming framework was used (Table 1) (Liu et al., 2017). This framework, based on Liu et al. (2017), includes a 13-year future climate sensitivity simulation with modified initial and boundary conditions set to the high-end, end-of-current-century emission scenario as averaged across 19 global climate models. The historical and future WRF simulations were first compared to generate a monthly delta value for air temperature, relative humidity and incoming longwave radiation; the 4-km data were downscaled to 2-m using nearest neighbour technique. The historical DHSVM forcing file was then perturbed by the respective WRF delta values to simulate future snow water storage and hydrologic partitioning across the study catchment and across the same timeframe as the historical simulation. In the future simulation, hourly air temperature values increased by an average 5°C (±1.1°C), hourly relative humidity changed by an average −2.8% (±7%), and hourly longwave radiation increased by an average 2.5 W/m² (±0.5 W/m²).

3.4 | Annual average SSI

To represent the continuum of snow water storage in the study catchment, we derived an annual average metric (i.e., a SSI) following the methodology of Hale, Jennings, et al. (2023). The SSI describes the difference in timing between when effective precipitation (rainfall or snowfall) occurs versus when water is available and delivered to the catchment as SWI (the hourly sum of rain and snowmelt). The SSI thus represents annual average differences between the phase and the amplitude of effective precipitation seasonality and SWI

seasonality, creating a dimensionless value between −1 (seasonal effective precipitation and SWI in-phase) and 1 (seasonal effective precipitation and SWI out-of-phase). An SSI value of 0 signifies no seasonality in effective precipitation and SWI (i.e., uniform temporal distribution). Annual average SSI values were calculated by building on the methodology outlined in Woods (2009), first generating an effective precipitation sine curve, subscript P :

$$P(t) = \bar{P} \left[1 + \delta_P \sin \left(\frac{2\pi(t - s_P)}{365} \right) \right], \quad (1)$$

where \bar{P} is the mean annual precipitation, t is the timestamp (days), s_P is a precipitation phase shift (days) and δ_P is the dimensionless seasonal amplitude of precipitation. Second, a SWI sine curve was developed, subscript SWI:

$$SWI(t) = \overline{SWI} \left[1 + \delta_{SWI} \sin \left(\frac{2\pi(t - s_{SWI})}{365} \right) \right], \quad (2)$$

where \overline{SWI} is the mean annual surface water inputs, t is the timestamp (days), s_{SWI} is a SWI phase shift (days) and δ_{SWI} is the dimensionless seasonal amplitude of SWI. To generate the SSI, the determined phase and amplitude from Equations 1 and 2 were mathematically related using a similarity index:

$$SSI = - \left[\delta_{SWI} \operatorname{sgn}(\delta_P) \cos \left(\frac{2\pi(s_{SWI} - s_P)}{365} \right) \right]. \quad (3)$$

‘Sgn’ represents the ‘sign’ function, which extracts the sign of a real number. The final calculations were multiplied by −1 to emphasize typical snow-water-storing behaviour as a positive value, greater than 0. During the analysis of historical and future SSI values, including SSI constituents (SWE, P and SWI), and hydrologic partitioning, the study domain was evaluated as an averaged whole, as individual 2 m grid cells, and as an average of grid cells with SSI >0 and an average of grid cells with SSI ≤0, a numerical threshold guided by previous

SSI analyses (Hale, Jennings, et al., 2023). We particularly focused on regions of the alpine catchment with an SSI >0, because these areas stored the majority of water in the snowpack across the catchment had the highest potential for SSI and hydrologic change under warming conditions.

3.5 | Budyko framework

We evaluated model-derived hydrologic partitioning metrics within the study catchment in the context of the Budyko framework (Budyko, 1974), with an emphasis on the annual average SSI as the primary independent variable controlling partitioning behaviour. The Budyko framework was selected based on its ability to normalize water partitioning across climates and the similar use of this framework across several highly related studies (e.g., Barnhart et al., 2016; Berghuijs et al., 2014; Hale, Musselman, et al., 2023; Liu et al., 2022). Partitioning of water, in this context, is defined as the annual fraction of effective precipitation (P) that becomes ET or Q. Evaporative demand is quantified as PET and not reference evaporation (Bjarke et al., 2023). To quantify annual hydrologic partitioning, we obtained DHSVM estimates of $\frac{PET}{P}$ and $\frac{ET}{P}$ for each grid cell and compared them to the respective expected values using the Budyko hypothesis (Figure 2). Due to significant spatial variability in effective P and SWE, from wind redistribution of snow, we expected equally large spatial variability in $\frac{PET}{P}$, $\frac{ET}{P}$ and $\frac{Q}{P}$ (estimated via $1 - \frac{ET}{P}$). The expected annual partitioning behaviour estimated from the Budyko framework was

obtained for each grid cell relating the aridity index (i.e., $\frac{PET}{P}$) to the evaporative index (i.e., $\frac{ET}{P}$):

$$\frac{ET_{expected}}{P_{expected}} = \sqrt{\left(\frac{PET}{P} \tanh\left(\frac{P}{PET}\right)\right) \left(1 - \exp\left(-\frac{PET}{P}\right)\right)}. \quad (4)$$

The Budyko framework thus served as the expected $\frac{ET}{P}$ (or $1 - \frac{Q}{P}$) value for any $\frac{PET}{P}$ value. Vertical annual average anomalies were calculated as follows:

$$\frac{ET_{anom}}{P} = \frac{ET_{expected}}{P_{expected}} - \frac{ET_{DHSVM}}{ET_{DHSVM}}. \quad (5)$$

Where $\frac{ET_{anom}}{P}$ was the vertical difference between the expected $\frac{ET}{P}$, per the Budyko hypothesis, and the $\frac{ET}{P}$ fraction from the DHSVM output. By comparing observed versus expected partitioning behaviour, the amount of annual effective precipitation that is partitioned to ET relative to an expectation was determined based on the relative water- and energy-limitation of a given modelled grid cell (Figure 2). Thus, anomalies from the Budyko hypothesis result from overproduction of either catchment Q or ET, and these grid cells fall below and above the line, respectively (Barnhart et al., 2016) (Figure 2). Water partitioning may change relative to the expectation, represented by the Budyko curve, depending on historical and future climate and snow water storage conditions (Hale, Musselman, et al., 2023). As such, we evaluated statistical regressions, stratified by land cover

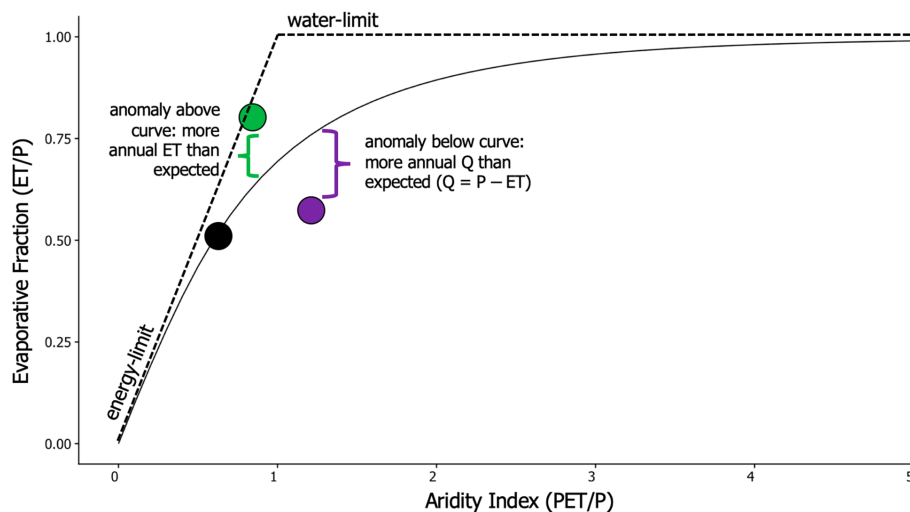


FIGURE 2 Hypothetical depiction of the Budyko framework (Budyko, 1974), used to predict the amount of annual effective precipitation (P), which will become evaporated (ET) or runoff (Q), based on an index of the catchment aridity ($\frac{PET}{P}$). The black line represents the Budyko expectation. Energy-limited catchments are classified as $\frac{PET}{P} < 1$, and water-limited catchments are classified as $\frac{PET}{P} > 1$. The black point represents a catchment, which partitions annual water inputs as expected. The green point represents a catchment, which partitions more water inputs to ET than expected, and the green bracket is the quantifiable annual average anomaly from the Budyko hypothesis. Finally, the purple point represents a catchment, which partitions more water inputs to Q than expected, and the purple bracket is the annual average anomaly from the expectation. To quantify anomalous behaviour, the vertical difference between the line and the point is taken (Equation 5). Thus, positive annual average anomaly values indicate points falling below the line (purple bracket) and thus more Q generated than expected, and negative annual average anomaly values indicate points falling above the line (green bracket) and thus less Q generated than expected.

type, between grid cell deviations from Budyko-expected $\frac{ET}{P}$ values and the annual average SSI to infer how water storage within snowpacks influences annual hydrologic partitioning behaviour, and to infer the sensitivity of hydrologic behaviour given the sensitivity of snowpack water storage to climate change.

3.6 | Monthly ratio of SWI and effective precipitation (SWI:P)

We used a monthly average of SWI:P as an additional independent environmental variable to compare against anomalies from the Budyko hypothesis. Because the annual average SSI is a function of P and SWI, a monthly SWI:P ratio provides first-principle and complementary insights into sub-annual snow water storage. Specifically, monthly SWI:P ratios greater than one indicate a release of snowpack water storage associated with snowmelt. Monthly SWI:P ratios less than one indicate an increase of water storage within the snowpack associated with snow accumulation. And a monthly SWI:P ratio equal to one indicates precipitation either fell as rain or melted soon after falling as snow. As such, we expected areas with greater annual average SSI values to experience smaller monthly SWI:P ratios in months corresponding with periods of storage of water in the snowpack, and large monthly SWI:P ratios when water was released from the snowpack during a significant snowmelt period. Conversely, areas with low annual average SSI values would experience larger monthly SWI:P ratios earlier in the year, corresponding to more rainfall or early season snowmelt, and smaller monthly SWI:P ratios later in the year when all snow had already melted in these areas.

The monthly SWI:P ratio analysis was originally conducted using a weekly timeframe, but we found that, ultimately, evaluating these variables by month was suitable in providing a first-principle explanation for water storage and release dynamics at the sub-annual scale. Months which showed weak or insignificant relationships ($r^2 < 0.3$ and/or $p > 0.05$) between the annual average SSI and the annual average Budyko anomaly throughout the water year were not further examined. Grid cells generating < 10 mm of SWI per average month were also excluded from the monthly SWI:P analysis.

4 | RESULTS

4.1 | Model testing

The selected historical simulation generated an $r^2 = 0.67$ and percent bias = 9.6% when comparing daily simulated runoff to the catchment stream gage from 2000 to 2019 (Bjarke et al., 2022). The optimal parameter values for the calibrated historical simulation are reported in Table 2. These parameter values were held consistent in the future simulation.

To further ensure conservation of mass, we evaluated catchment average daily precipitation, runoff, ET and sublimation to ensure that

TABLE 2 DHSVM parameters evaluated during the calibration phase of this work and the values selected for optimal model performance.

Model parameter	Units	Selected value
Lateral conductivity	No units	0.001
Exponential decay	No units	5
Snow water content	m/m	0.03
Maximum temperature at which snow occurs	°C	4.5

the model was adequately representing seasonal to annual hydrological fluxes (Figure S1). Averaged across 18 water years, error was < 10 mm. Annual average precipitation was 1033.7 mm, with 806.1 mm (78%) falling as snow between September and mid-June, consistent with a previous study of the catchment (Bjarke et al., 2021). The average fraction of precipitation that became runoff ($\frac{Q}{P}$) was 48%, which was similar to that of previous studies within this catchment that reported runoff ratios between 40% and 50% (Creed et al., 2014; Knowles et al., 2015). Thus, the results of our model testing efforts were deemed sufficient to move forward with the analysis.

4.2 | Effective precipitation and SWI

In the historical simulation, October through May was dominated by snowfall (88%–100% of monthly precipitation) and thus wind expectedly redistributed the solid precipitation, resulting in relatively more effective precipitation in the northwest and central portions of the study catchment. As a result, large snowdrifts formed in these areas, whereas less effective precipitation remained in the eastern region of the catchment (Figure S2a). However, in the future simulation, increased temperatures led to shifts from snowfall to rainfall in October and May and thus caused significant spatial changes in effective precipitation during these months across simulations (Figure 3; Figure S2a and S2b). With warming, there was a 77% and 91% decrease in snowfall in October and May, respectively. Smaller changes in snowfall fraction ($< 15\%$ decrease) and effective precipitation ($< 5\%$) between simulations occurred in November and April. December–March precipitation remained 100% snowfall in both scenarios, resulting in no changes in effective precipitation (Figure 3). Associated monthly changes in sublimation and ET were < 1 mm.

With warming, the decreased snowfall fraction and spatial heterogeneity of effective precipitation caused SWI generation to shift in time and space between historical and future simulations across the catchment, with snowmelt occurring an average 1 month earlier in the future, warming simulation (Figure 4). In the historical simulation, monthly SWI was 0 mm/month when precipitation was falling as snow in October through March (without snowmelt) but increased to a catchment average of 63 mm/month in April–July as the snowpack

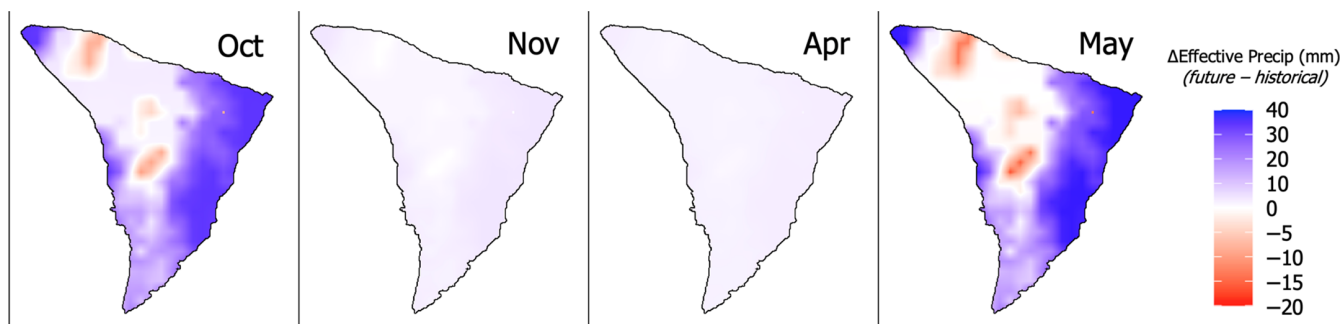


FIGURE 3 Differences in monthly average effective precipitation across the study catchment between the historical simulation and future simulation, during only months when effective precipitation did change between simulations. Purple shading represents increases in effective precipitation with warming, and white and red shading represents little change or decreases in effective precipitation with warming across simulations.

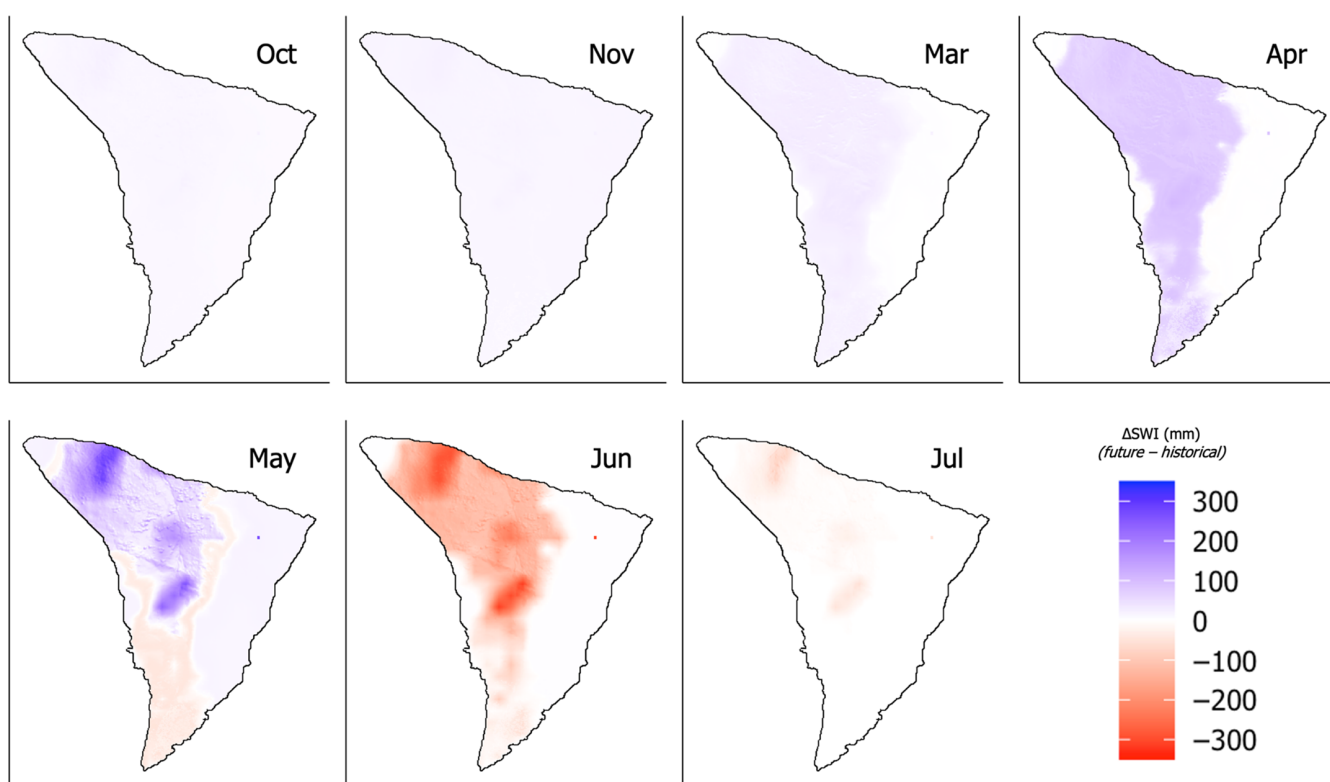


FIGURE 4 Differences in monthly average surface water inputs (SWI) across the study catchment between the historical simulation and future simulation, during only months when effective precipitation did change between simulations. Purple shading represents increases in SWI with warming, and white and red shading represents little change or decreases in SWI with warming across simulations.

melted (Figure S3a). The catchment sub-regions with snowdrifts generated the most monthly SWI during the snowmelt period (>300 mm/month). In contrast, the future simulation resulted in 0 mm/month of SWI from December through February, but SWI increased to a catchment average of 58 mm/month in March–June (Figure S3b). Thus, more catchment average SWI was generated in the future simulation in October, November and March–May, but substantially less SWI was generated in June and July. On average, snowmelt-generated SWI occurred one-month earlier in the future simulation than in the historical simulation (Figure 4). Further, in wind-scour regions, increases in rainfall fraction with warming resulted in SWI increases in

October, November and May, when there had previously been very little SWI generation in the historical simulation owing to wind-scouring of snow (Figure 4).

4.3 | Snow storage index

Changes in timing and magnitude of effective precipitation and SWI between historical and future simulations resulted in catchment average decreases in the SSI, with an average 57% decrease in SSI occurring in significant snow water storing areas with a positive SSI value

and snowdrifts (Figures 5, 6 and S4). More specifically, the wind redistribution of snowfall created significant differences in average annual SWE across the catchment and corresponding spatial differences in historical snow water storage. In the historical simulation, average annual SWE across the catchment was 53 mm, where areas with snowdrifts accumulated a maximum average annual 208 mm of SWE ($4\times$ the catchment mean) and wind-scoured regions accumulated a minimum average annual SWE of less than 1 mm, suggesting near zero snow coverage throughout the year (Figure 5a). In turn, the catchment average SSI was -0.07 in the historical simulation, with a grid cell SSI range of 0.84 in wind deposition areas with snowdrifts ($>10\times$ the mean) to -1 in wind-scoured regions of the catchment (Figure 5b). Thus, regions of the catchment with snowdrifts and positive SSI values were spatially similar to regions with significant SWE accumulation, and experienced highly seasonal effective precipitation and SWI, which were considerably out-of-phase with one another (average positive SSI grid cell shown in Figure 5c). On average, these areas experienced an annual SSI of 0.75.

Conversely, regions of the catchment with a small and negative SSI value experienced little annual SWE accumulation and thus less seasonal effective precipitation and SWI, which were in-phase with one another (average negative SSI grid cell shown in Figure 5d). On average, these areas experienced an annual SSI of -0.91 . Thus, the average catchment SSI was low because most of the catchment (84%) exhibits significant wind-scour of snow and thus small average SWE values (Figure 5a), which is the driver of temporal misalignment between precipitation and SWI. However, the remaining 16% of the catchment has historically experienced wind deposition of snow and a relatively large magnitude of effective precipitation, average annual SWE and SWI, which drastically misalign peak effective precipitation and peak SWI (Figure 5c). These areas with snowdrifts serve as substantial snow water storing regions within the catchment signifying the highest potential for change with future climate warming.

In contrast, in the future simulation, reduced wind redistribution of snowfall created reduced heterogeneity in average annual SWE

and snow water storage across the catchment. In the future simulation, average annual SWE across the catchment was 37 mm, where areas with snowdrifts accumulated a maximum average annual SWE of 158 mm (i.e., $4\times$ the catchment mean) and wind-scoured regions accumulated a minimum average annual SWE of less than 1 mm, suggesting consistent near zero snow coverage throughout the year (Figure 6a). In turn, the catchment average SSI was -0.11 in the future simulation, with a grid cell SSI range of 0.42 in areas with snowdrifts to -1 in wind-scour regions of the catchment (Figure 6b).

Regions of the catchment with a positive SSI value were spatially similar to regions with significant SWE accumulation in the future simulation. However, in comparison to the historical simulation, both the magnitude of seasonal effective precipitation and SWI, and the associated temporal misalignment, in positive SSI regions were decreased in the future simulation, (average positive SSI grid cell shown in Figure 6c). This resulted in 100% decreases in SSI occurring in regions with snowdrifts and a positive SSI value, suggesting a disproportionately large impact on the SSI with warming in considerable snow water storing regions of the alpine. On average, these areas experienced an annual SSI of 0.32. Conversely, regions of the catchment with a negative SSI value remained somewhat unchanged ($<5\%$ average difference) with little annual SWE accumulation and low seasonality in effective precipitation and SWI, which were in-phase with one another (average negative SSI grid cell shown in Figure 6d). On average, these areas experienced an annual SSI of -0.87 . In total, 92% of the catchment experienced a negative SSI in the future simulation, resulting in the negative catchment average SSI. Spatially distributed percent change in SSI is shown in Figure S4.

4.4 | Hydrologic partitioning

Contrasting changes in runoff with warming revealed differences in partitioning behaviour between positive and negative SSI regions of

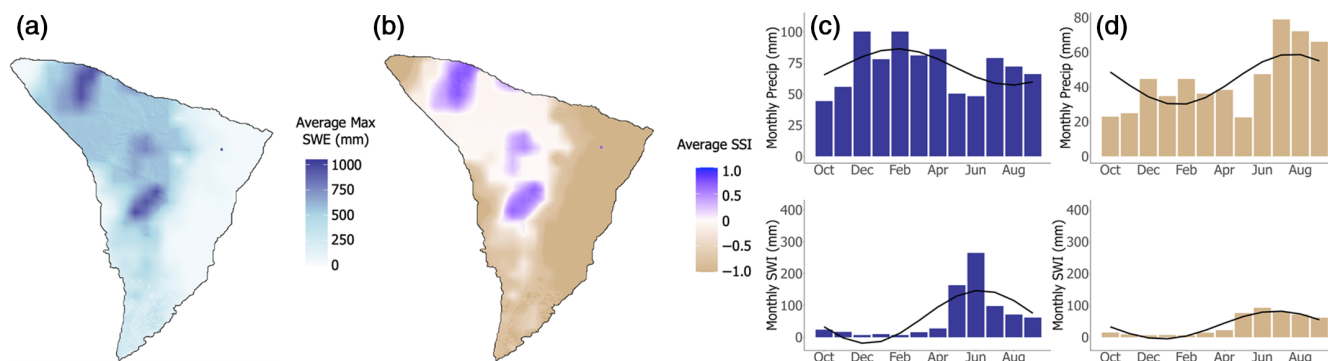


FIGURE 5 Historical simulation (a) average annual snow water equivalent (SWE) (mm) for each grid cell in the study catchment and (b) corresponding Snow Storage Index (SSI) values. Panel (c) shows the average monthly effective precipitation (mm, top) and SWI (mm, bottom) for all grid cells with a positive SSI value (purple grid cells in b). Panel (d) shows the average monthly effective precipitation (mm, top) and surface water inputs (SWI) (mm, bottom) for all grid cells with a negative SSI value (tan grid cells); note that in c and d corresponding seasonality curves are shown.

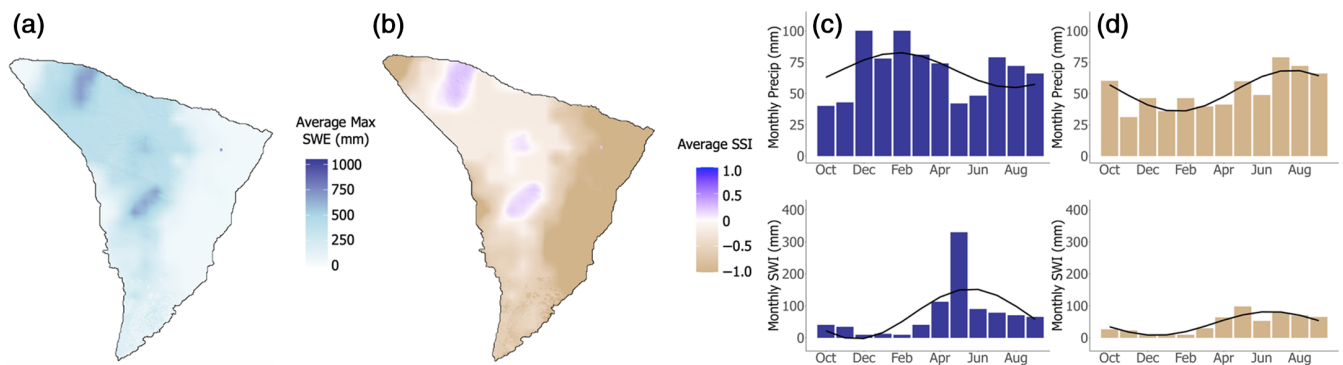


FIGURE 6 Future, warming simulation, (a) average annual snow water equivalent (SWE) (mm) for each grid cell in the study catchment, (b) corresponding Snow Storage Index (SSI) values. Panel (c) shows the average monthly effective precipitation (mm, top) and surface water inputs (SWI) (mm, bottom) for all grid cells with a positive SSI value (purple grid cells). Panel (d) shows the average monthly effective precipitation (mm, top) and SWI (mm, bottom) for all grid cells with a negative SSI value (tan grid cells); note that in c and d corresponding seasonality curves are shown.

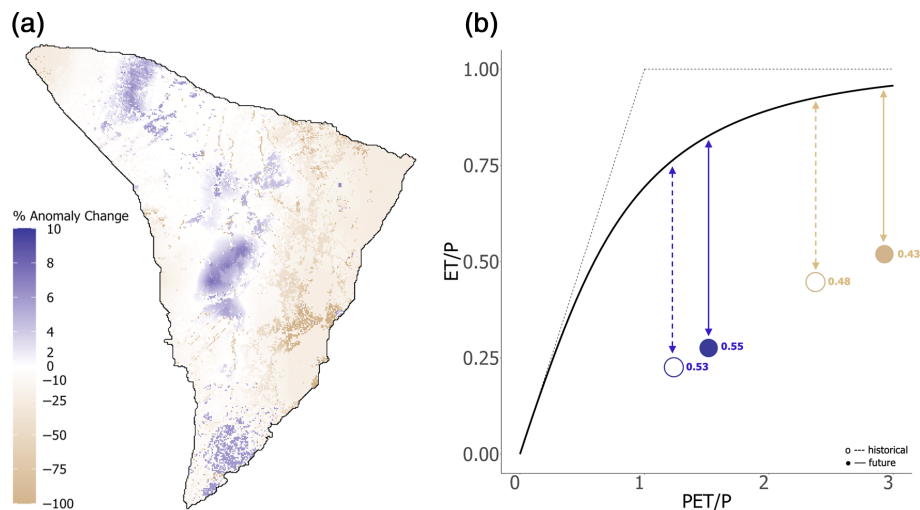


FIGURE 7 (a) Spatially distributed % change in annual average Budyko anomaly between the control and warming simulations. Purple shading indicates increases in partitioning of effective precipitation to runoff in the warming simulation, whereas white and tan shading indicates decreases in partitioning to runoff in the warming simulation, (b) Average $\frac{PET}{P}$ and $\frac{ET}{P}$ for all grid cells with a positive Snow Storage Index (SSI) value (purple grid cells) and 0 or negative SSI value (white and tan grid cells) in Budyko space with noted anomaly values for each simulation. The historical simulation is represented by an open circle and dashed line, and the future simulation is represented by a solid circle and solid line. The double-arrowheads represent the way in which anomaly values were calculated (y-value of black curve minus y-value of point).

the catchment, with continued disproportionately anomalous behaviour occurring in regions of the catchment with snowdrifts. First, evaluating the catchment under the Budyko hydrologic partitioning hypothesis, the catchment annual average Budyko anomaly was 0.50 in the historical simulation and 0.44 in the future simulation, resulting in an average 12% decrease in partitioning of effective precipitation to runoff from the expectation under warming. However, across the catchment by grid cell, the hydrologic partitioning response to a warming climate varied in direction and magnitude (Figure 7a). On average, in areas of the catchment with snowdrifts and where SSI was originally positive, aridity ($\frac{PET}{P}$) and evaporative ($\frac{ET}{P}$) indices were relatively low compared with areas with a negative SSI. Ultimately, the positive SSI

regions, signifying substantial snow water storage, generated an average Budyko anomaly of 0.53 in the historical simulation and 0.55 in the future simulation (Figure 7b). This partitioning result with warming indicates that, on average and in both simulations, areas with a positive SSI generated more runoff than expected from the Budyko hypothesis (i.e., points fall below the line and generate a positive anomaly value). And with warming, these areas experienced an average 4% increase—with a maximum grid cell 10% increase—in partitioning of effective precipitation to runoff (average positive SSI grid cell shown Figure 7b).

Conversely, wind-scoured areas of the catchment where SSI was originally negative generated an average Budyko anomaly of 0.48 in

the historical simulation and 0.43 in the future simulation. This partitioning result also reveals that, on average and in both simulations, areas with a negative SSI generated more runoff than expected from the Budyko hypothesis (i.e., points fall below the line). With warming, these areas experienced an average 10% decrease—with a maximum grid cell 100% decrease—in partitioning of effective precipitation to runoff (Figure 7b). Again, because the regions of the catchment with a negative SSI make up the majority (84%–92%) in both simulations, a catchment average decrease in hydrologic partitioning to runoff was seen. Thus, the relatively small increases in runoff partitioning in significant snow water storing regions of the catchment (i.e., areas with snowdrifts and a positive SSI) represent contrasting partitioning behaviour from the mean and likely reduced or buffered the overall runoff loss in annual catchment runoff, particularly as these sub-regions dramatically change with warming. A summary of all total, maximum and/or mean landscape, hydrologic flux and snowpack values and characteristics, across averaged positive and negative SSI regions of the catchment and the historical and future simulations, are listed in Table 3.

4.5 | Annual average SSI and hydrologic partitioning

To determine the influence of snow water storage and release on hydrologic partitioning across the catchment, we place emphasis on grid cells with an SSI >0 in the alpine meadow land cover type, since this vegetation type represents the majority of the catchment (~55%, Figure 8a). In these areas, there was a strong and negative relationship between annual average SSI and annual Budyko anomaly, indicating that decreases in annual average SSI led to increases in the annual average Budyko anomaly (i.e., more partitioning to runoff than expected). These relationships were strong in both historical and future simulations (Figure 8a); with an r^2 of 0.70 and 0.45, ($p < 0.05$) respectively.

Interestingly, the bare ground and closed shrub land cover types did not show a similar relationship between SSI and Budyko anomaly as that seen in the alpine meadowland cover type (Figure 8b,c). Further, open shrub and evergreen broadleaf forest land cover types showed insignificant ($p > 0.05$) relationships between the annual

TABLE 3 Annual average water balance, snow water storage, and hydrologic partitioning total, average, and/or maximum values for the averaged grid cells where SSI >0 and SSI ≤0. The following variables are reported for both historical and future simulations.

Variable	Historical SSI >0	Future SSI >0	Historical SSI ≤0	Future SSI ≤0
Spatial coverage (%)	16	8	84	92
Predominant land cover types	Bare ground, Alpine Meadow, Closed Shrub	Bare ground, Alpine Meadow, Closed Shrub	Alpine Meadow, Open Shrub, Evergreen Broadleaf	Alpine Meadow, Open Shrub, Evergreen Broadleaf
Monthly Effective Precip (mm)	72 (mean), 100 (max) 862 (annual sum)	69 (mean), 100 (max), 945 (annual sum)	44 (mean), 79 (max) 533 (annual sum)	54 (mean), 79 (max) 642 (annual sum)
Monthly SWE (mm)	143 (mean), 341 (max)	70 (mean), 149 (max)	56 (mean), 117 (max)	17 (mean), 39 (max)
Date of Max SWE	May 21	March 26	May 17	March 15
Snow-covered days	313	182	295	136
Monthly SWI (mm)	64 (mean), 265 (max) 768 (annual sum)	75 (mean), 330 (max) 895 (annual sum)	39 (mean), 93 (max) 462 (annual sum)	45 (mean), 81 (max) 539 (annual sum)
Annual ET/P	0.23	0.28	0.45	0.52
Annual PET/P	1.24	1.51	2.37	2.93
SSI	0.75	0.32	−0.91	−0.87
Budyko Anomaly	0.53	0.55	0.48	0.43

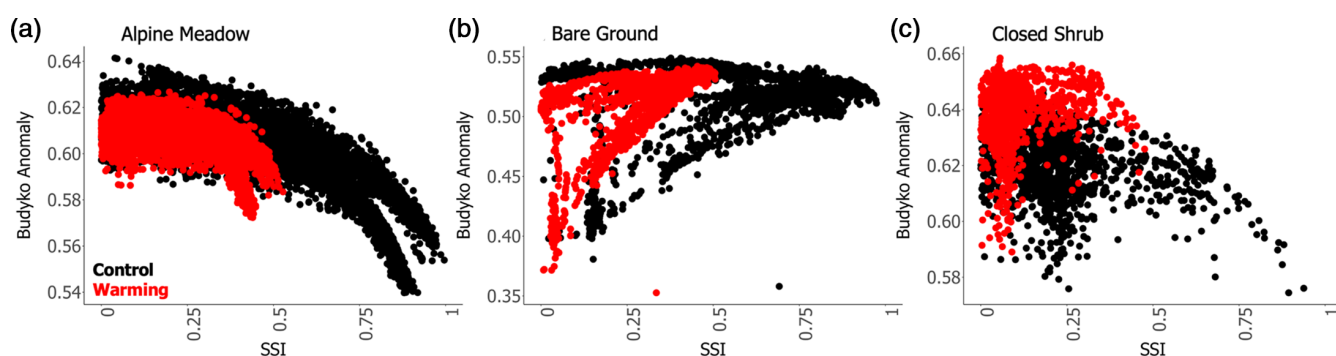


FIGURE 8 Grid cell scale annual average Snow Storage Index (unitless) regressed against the annual average Budyko anomaly (unitless) within the (a) bare ground, (b) alpine meadow and (c) closed shrub land cover types in the (black) historical simulation and (red) future simulation.

average SSI and the annual average Budyko anomaly (Figure S6). Such differences in the relationship shown in Figure 8 and Figure S6 shed light on different potential hydrologic mechanisms acting on the

catchment at one time. Further, this may also be related to decreased sample size, compared with the alpine meadow land cover type, sub-surface characteristics, increased overstory and understory density, or model treatment of canopy (see Section 5.3 and 5.4).

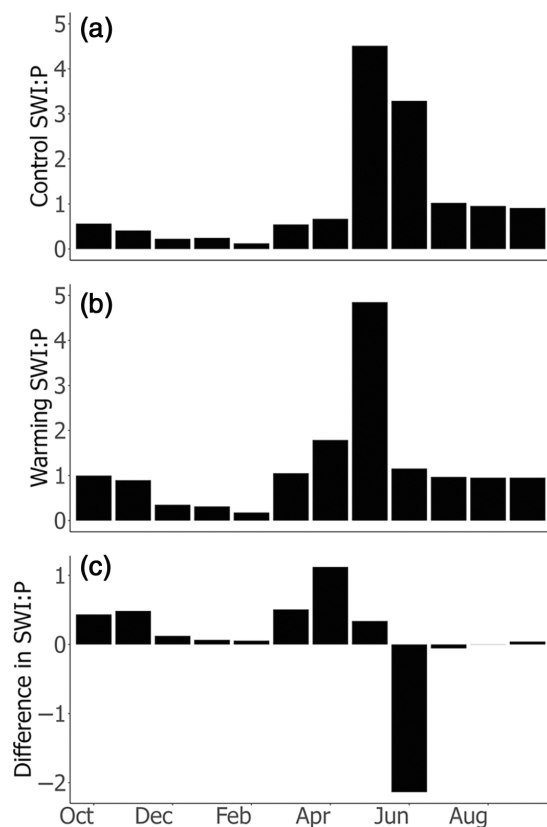


FIGURE 9 Monthly catchment average ratios of surface water input generation (rainfall + snowmelt) to precipitation (SWI:P) during the (a) historical simulation, and (b) future simulation, and the (c) difference in the monthly average SWI:P ratios between simulations. SWI, surface water inputs.

4.6 | Monthly SWI:P ratio and hydrologic partitioning

In the historical simulation, the catchment monthly average SWI:P ratio was <1 in October–March and >1 in May and June (Figure 9a). However, in the future, warming simulation, the catchment monthly average SWI:P ratio was ~ 1 in October–November and >1 in April and May (Figure 9b). To depict change across simulations, Figure 9c shows the difference in catchment monthly average SWI:P ratios, where a positive value (e.g., October through May) indicates the catchment monthly amount of SWI relative to catchment monthly precipitation increased in the future simulation. A negative value (e.g., June) indicates decreased June SWI relative to June precipitation in the future simulation. Thus, the vast majority of months showed reductions in the storage of water as snow with warming and instead increases in water release from the snowpack. Notably, these increases in winter and spring catchment monthly average SWI:P ratios were balanced by a very large decrease in monthly average SWI:P in June.

Spatially, in both simulations, the Budyko anomaly exhibited a statistically significant relationship with monthly SWI:P ($p < 0.05$ in all months) in the alpine meadowland cover type, particularly in areas where $SSI > 0$ and during periods of water storage (e.g., February, March and April), and water release (e.g., May and June) (Figure 10a). Notably, SWI:P incrementally increases throughout these months (i.e., magnitude of x-axis). In the historical simulation, the relationship between monthly SWI:P and average annual Budyko anomaly was positive in late winter and early spring months (e.g., February through

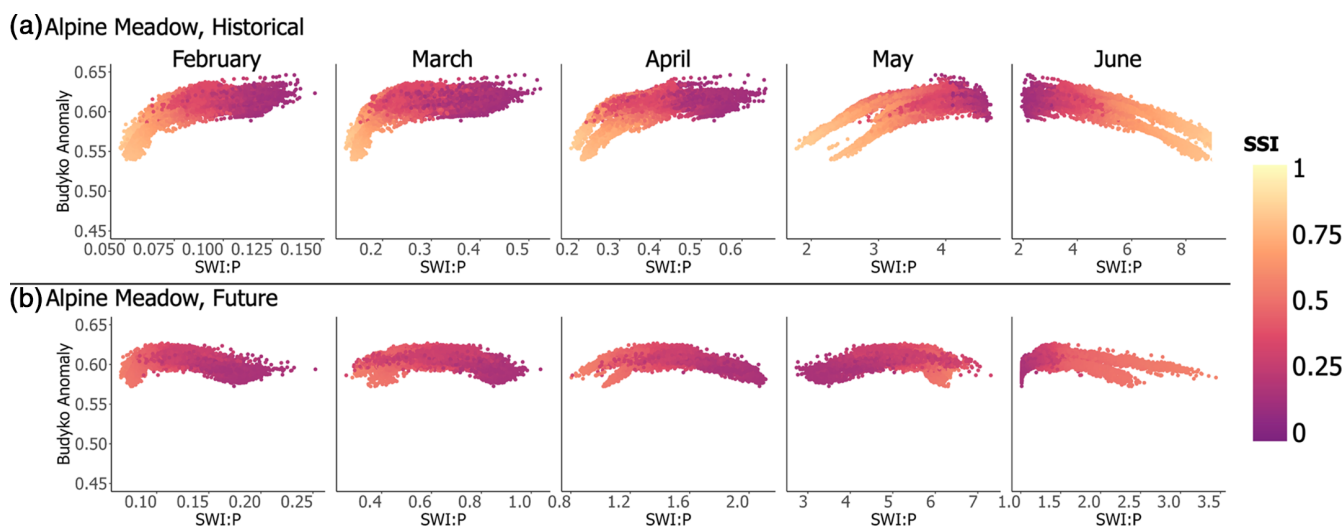


FIGURE 10 Grid cell scale monthly SWI:P ratios (unitless) regressed against the annual average Budyko anomaly (unitless), stratified by Snow Storage Index (SSI) values (>0) within the alpine meadowland cover type in the (a) historical simulation and (b) future simulation. SWI, surface water inputs.

May panels). In these months, the largest SWI:P ratios, corresponding with the smallest SSI values, and yielded the largest annual average Budyko anomalies (e.g., Figure 10a, February panel). In June, SWI:P reached its maximum in large SSI regions as the sign of the relationship changed from positive to negative (Figure 10a). And while the SWI:P was highest in large SSI areas experiencing significant snowmelt, these regions yielded the smallest annual average Budyko anomalies (e.g., Figure 10a, June). The relationships between monthly SWI:P and annual average Budyko anomaly persisted in the warming simulation (Figure 10b). With changes in the SWI:P ratio magnitude, the slope of the regression changed sign from positive to negative in the month of May—one month earlier than in the historical simulation—indicating earlier release of water from the snowpack in large SSI areas with warming.

Additional land cover types and all grid cells/SSI values are shown in Figures S7, S8 and S9. No statistically significant relationship ($p > 0.05$ in all months) existed between the monthly average SWI:P and the annual average Budyko anomaly in the evergreen broadleaf forest vegetation type (not shown), and or open shrub land cover type (Figure S10), suggesting added complexity in the SWI:P-Budyko anomaly relationship around forest canopies.

5 | DISCUSSION

5.1 | Snow storage index

Snow water storage, represented by the annual average SSI, is expected to decrease with climate warming due to shifts in the timing and magnitude of its components, effective precipitation and SWI (Hale, Jennings, et al., 2023). However, the impact that declines in snow water storage have on downstream partitioning of water to runoff or ET has remained relatively unknown, particularly at the alpine, headwater catchment scale and under future climate conditions (Hale, Musselman, et al., 2023). Our select alpine headwater catchment in the Rocky Mountains of Colorado, USA, represents the complete range of SSI values (−1 to 1), with extreme heterogeneity in snowpack accumulation and thus misalignment between seasonal precipitation and SWI. The extreme spatial variability of precipitation inputs, particularly of snowfall, is governed by the wind redistribution of snow, and the subsequent high degree of spatial heterogeneity in the hydrologic response to precipitation inputs makes the Saddle Catchment a compelling location to evaluate these fine scale relationships.

As the climate warms, lower elevations are experiencing more precipitation as rainfall and the snowpack is melting earlier in the year (Mote et al., 2018; Musselman et al., 2017, 2021). Given the relatively high elevation of the Saddle Catchment, the watershed has not yet experienced many of the expected hydrological consequences of warming (Jennings and Molotch, 2020). However, the end-of-century warming simulation conducted here illustrates the potential consequences of warming on snow water storage in areas prone to significant wind redistribution of snow, a characteristic feature of alpine environments. In turn, the effects of future precipitation phase shifts

towards more rainfall and less snowfall in the study area decreased the modelled spatial heterogeneity of effective precipitation throughout the year because snowfall was redistributed by wind whereas rainfall was not (Winstal et al., 2013). These changes drove a shift towards earlier SWI across the catchment (Figures 3, 4 and S2). Such changes in precipitation inputs and water availability created disproportionately large SSI decreases in snow water storing areas with snowdrifts, which decreased by 57% on average (Figures 6 and S4). The modelled changes in SSI are meaningful as they highlight the spatially disparate climate sensitivities between areas with positive SSI versus negative SSI.

5.2 | Hydrologic partitioning

With warming, the effect of rainfall occurring in autumn and spring months and snowmelt occurring earlier in spring when atmospheric demand was relatively low resulted in greater partitioning of effective precipitation to runoff in areas with SSI > 0 (average 4% increase). Thus, decreased effective precipitation and increase in SWI earlier in the year in the future simulation, brought on by warming and earlier snowmelt, may influence sub-catchment hydrology and increase partitioning of water inputs to runoff more than the corresponding influence from increased PET and ET that is commonly associated with warmer air temperatures (Mahanama et al., 2012; Tang & Lettenmaier, 2012). These results may be somewhat unique to alpine environments given the relatively thin soils, shallow rooting depths, and significant energy limitations relative lower elevation forested areas (Burns, 1980; Williams et al., 1996).

Interestingly, the 10% decrease in hydrologic partitioning to runoff with warming in historically negative SSI areas suggests that increases in water availability from more uniformly distributed rainfall—which acted to increase effective precipitation in these areas—did not exceed increases in evaporative demand associated with warming (Figure 7 and Table 3). Thus, overall partitioning to ET in these areas increased. In turn, increased alignment of SWI and PET in arid areas (e.g., wind-scoured, negative SSI areas) by way of increased fall and spring season rainfall with warming acted to decrease hydrologic partitioning to streamflow. This is consistent with previous work showing that changes in the energy budget and increased evaporative demand are more impactful on hydrologic partitioning in arid areas of the catchment than less arid regions (e.g., snowdrifts, positive SSI regions) (Foster et al., 2016). Catchment average and grid-cell changes in hydrologic partitioning to runoff with warming were also consistent with a previous study evaluating opposing mechanistic ‘perspectives’, which impact runoff differently across wet and dry years (water-i vs. water-ii in Liu et al., 2022). Quantifying the amount that a historical snowmelt pulse or varying temporal misalignment between water availability and evaporative demand regulate hydrologic partitioning in sub-regions of the study catchment was beyond the scope of this work. Future field-based studies are needed to investigate and quantify the hydrologic impact of these mechanisms (Fan et al., 2019; Wlostowski et al., 2021).

Because the study catchment has historically experienced ~80% of its annual precipitation in the form of snow (Bjarke et al., 2021), the potential changes in snow water storage and hydrologic partitioning characterized herein are important to potential ecological and biological stresses within and around the catchment and similar alpine areas globally (Wieder et al., 2022).

5.3 | SSI controls on hydrologic partitioning

On average, a larger catchment SSI in the historical simulation led to more partitioning of effective precipitation to runoff (Q) than in the future simulation. Similarly, model simulations show that for all land cover types, the average Budyko anomaly is far greater in areas with greater SSI (Figure S6). However, within sub-regions of the catchment storing >90% of the catchment water in the snowpack (i.e., SSI values >0), the relationship between SSI and annual average Budyko anomalies showed that larger SSI values partitioned less effective precipitation to runoff (Q) from the expected Budyko hypothesis compared with SSI values closer to 0 (Figure 8). This was particularly true in the alpine meadow land cover type ($p < 0.05$, $r^2 = 0.70$ and 0.45)—which represents the majority of the catchment area—indicating comparable and/or improved predictive power of the annual average SSI to water partitioning relative to previous works relating snowmelt rate (e.g., Barnhart et al., 2016, $r^2 = 0.9$ – 0.72), and snow fraction (e.g., Berghuijs et al., 2014, $r^2 = 0.30$) to the annual average Budyko anomaly.

The SSI-Budyko anomaly result is comparable to larger-scale work relating annual average SSI values to annual average Budyko anomalies across the western United States (e.g., Hale, Musselman, et al., 2023, $r^2 = 0.03$ – 0.62). However, this work additively suggests that sub-catchment scale impacts of SSI on hydrologic partitioning may differ depending on snowpack heterogeneity, potentially buffering catchment average losses in runoff. In the future, positive SSI values are related to increased partitioning of annual precipitation inputs to runoff from the Budyko expectation. This suggests that the temporal misalignment between water availability earlier in the year (i.e. increased winter and early spring SWI with warming) and atmospheric demand in warmer, summer months (i.e. increased summer PET with warming) is an important determinant of hydrologic sensitivity to warming (Barnhart et al., 2016; Foster et al., 2016; Hale, Musselman, et al., 2023). Moreover, the different partitioning responses to warming across land cover types and positive versus negative SSI regions and historically versus in the future—across a single catchment—represent a potential paradox in the snow water storage and annual runoff partitioning relationship (Figures 8, S7, S8 and S9). Further consideration is needed to disentangle the drivers of hydrologic partitioning characteristics across spatially heterogeneous alpine catchments like the Saddle Catchment.

Alpine headwater areas like the Saddle Catchment provide the majority of downstream water resources in many semi-arid mountainous regions of the globe (Beniston & Stoffel, 2014; Knowles et al., 2015). The results herein carry significant implications for

understanding climate-related changes to runoff production and the associated spatial complexity of these changes. As warming and changes in precipitation phase continue (Ikeda et al., 2021), areas with significant snowdrifts may produce proportionally more runoff than they have historically but catchment-average proportional runoff may decrease. In addition to the important considerations of these potential changes for water resources, these changes may also effect spatio-temporal variability in soil moisture, groundwater recharge, plant productivity and nutrient cycling (Kormos et al., 2014; McNamara et al., 2005).

5.4 | Limitations

The SWE reconstruction model—which provided the basis for snowfall distribution—relied on satellite imagery for snow cover information (Jepsen et al., 2012) which has less reliability below forest canopy cover. However, because forest cover makes up only 3.6% of the study area, we expect these limitations to be small and isolated.

We limited the warming perturbations to air temperature, relative humidity and incoming longwave radiation. Across the historical and future simulations, we held historical precipitation constant, only allowing for changes in effective precipitation due to differences in phase (snowfall vs. rainfall). Allowing precipitation amount to change would have eliminated a means of deciphering how changes in SSI impact ET and runoff, as changes in precipitation would have also impacted annual partitioning (Brooks et al., 2015; Kalra & Ahmad, 2011; Kittel et al., 2015). The annual average projected change in precipitation in the catchment was small, with an annual average +6.7% (October–April = +8.5%; May–September = +3.3%) (Liu et al., 2017). Future increases in precipitation would expectedly alter the timing and amount of water availability from the catchment, the annual average SSI, and monthly SWI:P.

While land cover, soil and subsurface characteristics were held constant across simulations in this work, it is likely that the long-term distribution of land cover classification will change with warming (Brooks et al., 2015). As such, it is expected that the extent of tree line may expand to higher latitudes and elevations (Brooks et al., 2015), and it is known that shrubs are increasing in this area (Bueno de Mesquita et al., 2018). Increased shrubs and forest cover could increase snow retention and decrease blowing snow while also increasing ET (Barnhart et al., 2021; Bueno de Mesquita et al., 2018). Subsequently, decreases in wind redistribution of snow would further reduce snowdrifting, which is currently critical in storing snow until later in the year and producing SWI in spring and summer months. Thus, with expected changes in land cover type across the study area to include more canopy cover (not currently represented in this study), seasonal and annual ET and Q will likely also change in the future, increasing or decreasing due to a variety of landscape processes and environmental interactions.

Lastly, the scale and accuracy of precipitation forcing data may have dramatic impacts on runoff simulation accuracy. Even at smaller catchment scales, spatial variability of precipitation has been shown to translate into large variations in modelled runoff (Faurès

et al., 1995; Goodrich et al., 1995). Limitations may be addressed in future work with higher resolution precipitation data and/or including a longer simulation period, which may enhance the initial model calibration process.

6 | CONCLUSION

This study addresses critical knowledge gaps in alpine hydrology by quantifying the spatial complexity of alpine snow water storage characteristics, how they are changing with time, and quantifying the mechanism by which snow water storage affects hydrologic partitioning. In this context, there are three important findings: First, we show that warming causes the SSI to decrease in snowdrift areas (average -57%) and increase in wind-scour areas (average $+4\%$). Decreases in snow water storage in positive SSI regions with snowdrifts were due to increased proportional rainfall and earlier snowmelt timing, indicating reduced storage of water in the snowpack for a shorter period of time in the future. Second, we show that the SSI explains up to 70% of the variability in the Budyko anomaly across most of an alpine headwater catchment ($r^2 = 0.70$; $p < 0.05$), which is significantly greater than previous studies performed at larger scales. This is an important result as it implies that the SSI may provide an important avenue to further explore mechanisms governing hydrologic partitioning. Third, we show that the partitioning response to warming is opposite in snowdrifts (i.e., $SSI > 0$) versus wind-scour areas (i.e., $SSI < 0$) whereby the Budyko anomaly increased by an average 4% in snowdrift areas but decreased by an average 10% in wind-scour areas. This result suggests that, in snowdrift areas, an increased temporal misalignment between water availability (i.e., SWI) and water demand (i.e., PET) with warming will drive increases in runoff in the areas most sensitive to warming. Conversely, wind-scour areas may see increased partitioning to ET with warming given that increases in SWI in these areas are unlikely to exceed soil moisture field capacities, as required for runoff generation. This differential response may be associated with the distinct energy-limited versus water-limited characteristics of snowdrift versus wind-scour regions, respectively. In this context, areas storing more water as snow ($SSI > 0$) partitioned proportionally more water to runoff than areas with less snow water storage regions ($SSI \leq 0$). Yet as annual catchment average SSI decreases with future warming, the partitioning of effective precipitation to runoff is expected to exhibit spatially heterogeneous impacts on runoff partitioning. The contrasting hydrologic sensitivities to warming between areas with snowdrifts versus those that are wind-scoured are important in the context of downstream water resources and the hydrology, ecology and biogeochemistry of alpine systems.

ACKNOWLEDGEMENTS

This research has been supported by the National Science Foundation [SPVKK1RC2MZ3], the National Oceanic and Atmospheric Administration [NA15OAR4310144], the National Aeronautics and Space Administration [NNX17AF50G, 80NSSC17K0071, 80NSSC20K1420], and the Western Water Assessment [NA21OAR4310309].

DATA AVAILABILITY STATEMENT

All historical and future model simulation outputs are publicly available via the EDI Data Portal: <https://doi.org/10.6073/pasta/15d8d9a6725b04efe32a4b839582a5d4>.

ORCID

Nels R. Bjarke  <https://orcid.org/0000-0002-0006-1060>

Eve-Lyn S. Hinckley  <https://orcid.org/0000-0002-7081-0530>

REFERENCES

- Anghileri, D., Voisin, N., Castelletti, A., Pianosi, F., Nijssen, B., & Lettenmaier, D. (2016). Value of long-term streamflow forecasts to reservoir operations for water supply in snow-dominated river catchments. *Water Resources Research*, 52, 4209–4225.
- Badger, A. M., Bjarke, N., Molotch, N. P., & Livneh, B. (2021). The sensitivity of runoff generation to spatial snowpack uniformity in an alpine watershed: Green Lakes valley, Niwot Ridge long-term ecological research station. *Hydrological Processes*, 35(9), e14331.
- Barnett, T. P., Adam, J. C., & Lettenmaier, D. P. (2005). Potential impacts of a warming climate on water availability in snow-dominated regions. *Nature*, 438, 303–309.
- Barnhart, T. B., Molotch, N. P., Livneh, B., Harpold, A. A., Knowles, J. F., & Schneider, D. (2016). Snowmelt rate dictates streamflow. *Geophysical Research Letters*, 43, 8006–8016.
- Barnhart, T. B., Vukomanovic, J., Bourgeron, P., & Molotch, N. P. (2021). Future land cover and climate may drive decreases in snow wind-scour and transpiration, increasing streamflow at a Colorado, USA headwater catchment. *Hydrological Processes*, 35(11), e14416.
- Baron, J., & Denning, A. S. (1993). The influence of mountain meteorology on precipitation chemistry at low and high elevations of the Colorado front range, USA. *Atmospheric Environment. Part A. General Topics*, 27(15), 2337–2349.
- Barry, R. G. (1973). A climatological transect on the east slope of the front range, Colorado. *Arctic and Alpine Research*, 5(2), 89–110.
- Beniston, M., & Stoffel, M. (2014). Assessing the impacts of climatic change on mountain waterresources. *Science of the Total Environment*, 493, 1129–1137.
- Berghuijs, W., Woods, R., & Hrachowitz, M. (2014). A precipitation shift from snow towardsrain leads to a decrease in streamflow. *Nature Climate Change*, 4, 583–586.
- Burns, S. F. (1980). *Alpine soil distribution and development, Indian Peaks, Colorado Front Range*. Ph.D. thesis. University of Colorado.
- Bilish, S. P., Callow, J. N., McGrath, G. S., & McGowan, H. A. (2019). Spatial controls on the distribution and dynamics of a marginal snowpack in the Australian Alps. *Hydrological Processes*, 33(12), 1739–1755.
- Bjarke, N., Barsugli, J., & Livneh, B. (2023). Ensemble of CMIP6 derived reference and potential evapotranspiration with radiative and advective components. *Scientific Data*, 10(1), 417.
- Bjarke, N., Hale, K., & Niwot Ridge LTER. (2022). Saddle catchment Distributed Hydrology Soil Vegetation Model simulation (DHSVM) surface variable outputs (SWE, snowmelt, streamflow, soil moisture), 2 meter, 2000–2019. ver 1. Environmental Data Initiative. [10.6073/pasta/15d8d9a6725b04efe32a4b839582a5d4](https://doi.org/10.6073/pasta/15d8d9a6725b04efe32a4b839582a5d4)
- Bjarke, N. R., Livneh, B., Elmendorf, S. C., Molotch, N. P., Hinckley, E. L. S., Emery, N. C., Johnson, P. T., Morse, J. F., & Suding, K. N., (2021). Catchmentscale observations at the Niwot Ridge long-term ecological research site. *Hydrological Processes*, 35(9), e14320.
- Blöschl, G., Kirnbauer, R., & Gutknecht, D. (1991). Distributed snowmelt simulations in an alpine catchment: 1. Model evaluation on the basis of snow cover patterns. *Water Resources Research*, 27(12), 3171–3179.
- Blöschl, G. Ö., & Kirnbauer, R. (1992). An analysis of snow cover patterns in a small alpine catchment. *Hydrological Processes*, 6(1), 99–109.

- Bowman, W. D. (1992). Inputs and storage of nitrogen in winter snowpack in an alpine ecosystem. *Arctic and Alpine Research*, 24(3), 211–215.
- Bowman, W. D., & Seastedt, T. R. (2001). *Structure and function of an alpine ecosystem: Niwot Ridge, Colorado*. Oxford University Press.
- Brandt, W. T., Bormann, K. J., Cannon, F., Deems, J. S., Painter, T. H., Steinhoff, D. F., & Dozier, J. (2020). Quantifying the spatial variability of a snowstorm using differential airborne lidar. *Water Resources Research*, 56(3), e2019WR025331.
- Brooks, E. S., Boll, J., & McDaniel, P. S. (2004). A hillslope-scale experiment to measure later saturated hydraulic conductivity. *Water Resources Research*, 40, WO4208. <https://doi.org/10.1029/2003WR002858>. 2004
- Brooks, P. D., Chorover, J., Fan, Y., Godsey, S. E., Maxwell, R. M., McNamara, J. P., & Tague, C. (2015). Hydrological partitioning in the critical zone: Recent advances and opportunities for developing transferable understanding of water cycle dynamics. *Water Resources Research*, 51(9), 6973–6987.
- Budyko, M. I. (1974). *Climate and life*. Academic Press.
- Bueno de Mesquita, C. P., Tillmann, L. S., Bernard, C. D., Rosemond, K. C., Molotch, N. P., & Suding, K. N. (2018). Topographic heterogeneity explains patterns of vegetation response to climate change (1972–2008) across a mountain landscape, Niwot Ridge, Colorado. *Arctic, Antarctic, and Alpine Research*, 50(1), e1504492.
- Caine, N. (1995). Temporal trends in the quality of Streamwater in an alpine environment: Green Lakes valley, Colorado front range, U.S.A. *Geografiska Annaler: Series A, Physical Geography*, 77(4), 207–220. <https://doi.org/10.1080/04353676.1995.11880441>
- Caine, T., Morse, J., & Niwot Ridge, L. T. E. R. (2023). Streamflow data for saddle stream, 1999 -ongoing. ver 8. Environmental Data Initiative. [10.6073/pasta/7de15f073c80e868423bf81970d2d5a0](https://doi.org/10.6073/pasta/7de15f073c80e868423bf81970d2d5a0)
- Campbell, D. H., Clow, D. W., Ingersoll, G. P., Mast, M. A., Spahr, N. E., & Turk, J. T. (1995). Processes controlling the chemistry of two snow-melt-dominated streams in the Rocky Mountains. *Water Resources Research*, 31(11), 2811–2821.
- Clow, D. W. (2010). Changes in the timing of snowmelt and streamflow in Colorado: A response to recent warming. *Journal of Climate*, 23(9), 2293–2306. <https://doi.org/10.1175/2009JCLI2951.1>
- Clow, D. W., Schrott, L., Webb, R., Campbell, D. H., Torizzo, A., & Dornblaser, M. (2003). Ground water occurrence and contributions to streamflow in an alpine catchment, Colorado front range. *Groundwater*, 41(7), 937–950.
- Creed, I. F., Spargo, A. T., Jones, J. A., Buttle, J. M., Adams, M. B., Beall, F. D., Booth, E. G., Campbell, J. L., Clow, D., Elder, K., Green, M. B., Grimm, N. B., Miniati, C., Ramlal, P., Saha, A., Sebestyen, S., Spittlehouse, D., Sterling, S., Williams, M. W., ... Yao, H. (2014). Changing forest water yields in response to climate warming: Results from long-term experimental watershed sites across North America. *Global Change Biology*, 20(10), 3191–3208.
- Currier, W. R., Sun, N., Wigmosta, M., Cristea, N., & Lundquist, J. D. (2022). The impact of forest-controlled snow variability on late-season streamflow varies by climatic region and forest structure. *Hydrological Processes*, 36(6), e14614.
- Fan, X., Gu, Y., Liou, K. N., Lee, W. L., Zhao, B., Chen, H., & Lu, D. (2019). Modeling study of the impact of complex terrain on the surface energy and hydrology over the Tibetan Plateau. *Climate dynamics*, 53, 6919–6932.
- Faurès, J. M., Goodrich, D. C., Woolhiser, D. A., & Sorooshian, S. (1995). Impact of small-scale spatial rainfall variability on runoff modeling. *Journal of Hydrology*, 173(1–4), 309–326.
- Foster, L. M., Bearup, L. A., Molotch, N. P., Brooks, P. D., & Maxwell, R. M. (2016). Energy budget increases reduce mean streamflow more than snow–rain transitions: Using integrated modeling to isolate climate change impacts on Rocky Mountain hydrology. *Environmental Research Letters*, 11(4), 044015. <https://doi.org/10.1088/1748-9326/11/4/044015>
- Freudiger, D., Kohn, I., Seibert, J., Stahl, K., & Weiler, M. (2017). Snow redistribution for the hydrological modeling of alpine catchments. *Wiley Interdisciplinary Reviews: Water*, 4(5), e1232.
- Goodrich, D. C., Faurès, J. M., Woolhiser, D. A., Lane, L. J., & Sorooshian, S. (1995). Measurement and analysis of small-scale convective storm rainfall variability. *Journal of Hydrology*, 173(1–4), 283–308.
- Greenland, D. (1989). The climate of Niwot Ridge, front range, Colorado, U.S.A. *Arctic and Alpine Research*, 21(4), 380. <https://doi.org/10.2307/1551647>
- Griessinger, N., Schirmer, M., Helbig, N., Winstral, A., Michel, A., & Jonas, T. (2019). Implications of observation-enhanced energy-balance snowmelt simulations for runoff modeling of alpine catchments. *Advances in Water Resources*, 133, 103410.
- Hammond, J. C., Saavedra, F. A., & Kampf, S. K. (2018). Global snow zone maps and trends in snow persistence 2001–2016. *International Journal of Climatology*, 38(12), 4369–4383.
- Hale, K. E., Jennings, K. S., Musselman, K. N., Livneh, B., & Molotch, N. P. (2023). Recent decreases in snow water storage in western North America. *Communications Earth & Environment*, 4(1), 170.
- Hale, K. E., Musselman, K. N., Newman, A. J., Livneh, B., & Molotch, N. P. (2023). Effects of snow water storage on hydrologic partitioning across the mountainous, western United States. *Water Resources Research*, 59, e2023WR034690. <https://doi.org/10.1029/2023WR034690>
- Hale, K. E., Wlostowski, A. N., Badger, A. M., Musselman, K. N., Livneh, B., & Molotch, N. P. (2022). Modeling streamflow sensitivity to climate warming and surface water inputs in a montane catchment. *Journal of Hydrology: Regional Studies*, 39, 100976.
- Harpold, A., Brooks, P., Rajagopal, S., Heidbuchel, I., Jardine, A., & Stielstra, C. (2012). Changes in snowpack accumulation and ablation in the intermountain west. *Water Resources Research*, 48(11), W11501. <https://doi.org/10.1029/2012WR011949>
- Hermes, A. L., Wainwright, H. M., Wigmore, O., Falco, N., Molotch, N. P., & Hinckley, E.-L. S. (2020). From patch to catchment: A statistical framework to identify and map soil moisture patterns across complex alpine terrain. *Frontiers in Water*, 2, 578602. <https://doi.org/10.3389/frwa.2020.578602>
- Hinckley, E., Ebel, B. A., Barnes, R. T., Anderson, R. S., Williams, M. W., & Anderson, S. P. (2012). Aspect control of water movement on hill-slopes near the rain-snow transition of the Colorado front range. *Hydrological Processes*, 28, 74–85. <https://doi.org/10.1002/hyp.9549>
- Horton, J. D. (2017). The state geologic map compilation (SGMC) geodatabase of the conterminous United States.
- Ikeda, K., Rasmussen, R., Liu, C., Newman, A., Chen, F., Barlage, M., Gutmann, E., Dudhia, J., Dai, A., Luce, C., & Musselman, K. (2021). Snowfall and snowpack in the Western US as captured by convection permitting climate simulations: Current climate and pseudo global warming future climate. *Climate Dynamics*, 57(7), 2191–2215.
- Immerzeel, W. W., Lutz, A. F., Andrade, M., Bahl, A., Biemans, H., Bolch, T., Hyde, S., Brumby, S., Davies, B. J., Elmore, A. C., Emmer, A., Feng, M., Fernández, A., Haritashya, U., Kargel, J. S., Koppes, M., Kraaijenbrink, P. D. A., Kulkarni, A. V., Mayewski, P. A., ... Baillie, J. E. M. (2020). Importance and vulnerability of the world's water towers. *Nature*, 577, 364–369. <https://doi.org/10.1038/s41586-019-1822-y>
- Jenicek, M., Seibert, J., & Staudinger, J. (2018). Modeling of future changes in seasonal snowpack and impacts on summer low flows in alpine catchments. *Water Resources Research*, 54(1), 538–556.
- Jennings, K. S., & Molotch, N. P. (2019). The sensitivity of modeled snow accumulation and melt to precipitation phase methods across a climatic gradient. *Hydrology and Earth System Sciences*, 23(9), 3765–3786.
- Jennings, K. S., & Molotch, N. P. (2020). Snowfall fraction, cold content, and energy balance changes drive differential response to simulated

- warming in an alpine and subalpine snowpack. *Frontiers in Earth Science*, 8, 186.
- Jennings, K., Kittel, T., Molotch, N., & Yang, K. (2021). Infilled climate data for C1, saddle, and D1, 1990–2019, hourly. ver 2. Environmental Data Initiative. [10.6073/pasta/Obf785f2f77c3f558f633853a4465404](https://doi.org/10.6073/pasta/Obf785f2f77c3f558f633853a4465404)
- Jepsen, S. M., Molotch, N. P., Williams, M. W., Rittger, K. E., & Sickman, J. O. (2012). Interannual variability of snowmelt in the Sierra Nevada and Rocky Mountains, United States: Examples from two alpine watersheds. *Water Resources Research*, 48(2). <https://doi.org/10.1029/2011WR011006>
- Jones, H. G. (Ed.). (2001). *Snow ecology: An interdisciplinary examination of snow-covered ecosystems*. Cambridge University Press.
- Kalra, A., & Ahmad, S. (2011). Evaluating changes and estimating seasonal precipitation for the Colorado River basin using a stochastic nonparametric disaggregation technique. *Water Resources Research*, 47(5).
- Kattelmann, R., & Elder, K. (1991). Hydrologic characteristics and water balance of an alpine basin in the Sierra Nevada. *Water Resources Research*, 27(7), 1553–1562.
- Kerkez, B., Glaser, S. D., Bales, R. C., & Meadows, M. W. (2012). Design and performance of a wireless sensor network for catchment-scale snow and soil moisture measurements. *Water Resources Research*, 48(9).
- Kittel, T. G., Williams, M. W., Chowanski, K., Hartman, M., Ackerman, T., Losleben, M., & Blanken, P. D. (2015). Contrasting long-term alpine and subalpine precipitation trends in a mid-latitude north American mountain system, Colorado front range, USA. *Plant Ecology & Diversity*, 8(5–6), 607–624.
- Knowles, J. F., Blanken, P. D., & Williams, M. W. (2015). Soil respiration variability across a soil moisture and vegetation community gradient within a snow-scoured alpine meadow. *Biogeochemistry*, 125(2), 185–202.
- Knowles, N., Dettinger, M. D., & Cayan, D. R. (2006). Trends in snowfall versus rainfall in the Western United States. *Journal of Climate*, 19(18), 4545–4559.
- Kormos, P. R., Marks, D., McNamara, J. P., Marshall, H. P., Winstral, A., & Flores, A. N. (2014). Snow distribution, melt and surface water inputs to the soil in the mountain rain-snow transition zone. *Journal of Hydrology*, 519, 190–204. <https://doi.org/10.1016/j.jhydrol.2014.06.051>
- Liu, C., Ikeda, K., Rasmussen, R., Barlage, M., Newman, A. J., Prein, A. F., Chen, F., Chen, L., Clark, M., Dai, A., Dudhia, J., Eidhammer, T., Gochis, D., Gutmann, E., Kurkute, S., Li, Y., Thompson, G., & Yates, D. (2017). Continental-scale convection-permitting modeling of the current and future climate of North America. *Climate Dynamics*, 49, 71–95. <https://doi.org/10.1007/s00382-016-3327-9>
- Liu, Z., Wang, T., Han, J., Yang, W., & Yang, H. (2022). Decreases in mean annual streamflow and interannual streamflow variability across snow-affected catchments under a warming climate. *Geophysical Research Letters*, 49(3), e2021GL097442.
- Livneh, B., & Badger, A. M. (2020). Drought less predictable under declining future snowpack. *Nature Climate Change*, 10, 452–458. <https://doi.org/10.1038/s41558-020-0754-8>
- Livneh, B., Deems, J., Buma, B., Barsugli, J., Schneider, D., Molotch, N., Wolter, K., & Wessman, C. A. (2015). Catchment response to bark beetle outbreak and dust-on-snow in the Colorado Rocky Mountains. *Journal of Hydrology*, 523, 196–210. <https://doi.org/10.1016/j.jhydrol.2015.01.039>
- Livneh, B., Deems, J. S., Schneider, D., Barsugli, J. J., & Molotch, N. P. (2014). Filling in the gaps: Inferring spatially distributed precipitation from gauge observations over complex terrain. *Water Resources Research*, 50(11), 8589–8610.
- López-Moreno, J. I., Fassnacht, S. R., Beguería, S., & Latron, J. B. P. (2011). Variability of snow depth at the plot scale: Implications for mean depth estimation and sampling strategies. *The Cryosphere*, 5(3), 617–629.
- López-Moreno, J. I., Fassnacht, S. R., Heath, J. T., Musselman, K. N., Revuelto, J., Latron, J., Morán-Tejeda, E., & Jonas, T. (2013). Small scale spatial variability of snow density and depth over complex alpine terrain: Implications for estimating snow water equivalent. *Advances in Water Resources*, 55, 40–52.
- Mahanama, S., Livneh, B., Koster, R., Lettenmaier, D., & Reichle, R. (2012). Soil moisture, snow, and seasonal streamflow forecasts in the United States. *Journal of Hydrometeorology*, 13, 189–203.
- Marks, D., & Winstral, A. (2001). Comparison of snow deposition, the snow cover energy balance, and snowmelt at two sites in a semiarid mountain basin. *Journal of Hydrometeorology*, 2(3), 213–227.
- Marshall, A. M., Link, T. E., Abatzoglou, J. T., Flerchinger, G. N., Marks, D. G., & Tedrow, L. (2019). Warming alters hydrologic heterogeneity: Simulated climate sensitivity of hydrology-based microrefugia in the snow-to-rain transition zone. *Water Resources Research*, 55(3), 2122–2141.
- Mazzotti, G., Currier, W. R., Deems, J. S., Pflug, J. M., Lundquist, J. D., & Jonas, T. (2019). Revisiting snow cover variability and canopy structure within forest stands: Insights from airborne lidar data. *Water Resources Research*, 55(7), 6198–6216.
- McNamara, J. P., Chandler, D., Seyfried, M., & Achet, S. (2005). Soil moisture states, lateral flow, and streamflow generation in a semi-arid, snowmelt-driven catchment. *Hydrological Processes: An International Journal*, 19(20), 4023–4038.
- Mote, P. W., Li, S., Lettenmaier, D. P., Xiao, M., & Engel, R. (2018). Dramatic declines in snowpack in the western US. *Npj Climate and Atmospheric Science*, 1, 2. <https://doi.org/10.1038/s41612-018-0012-1>
- Mott, R., Vionnet, V., & Grünwald, T. (2018). The seasonal snow cover dynamics: Review on wind-driven coupling processes. *Frontiers in Earth Science*, 6, 197.
- Musselman, K. N., Addor, N., Vano, J. A., & Molotch, N. P. (2021). Winter melt trends portend widespread declines in snow water resources. *Nature Climate Change*, 11(5), 418–424.
- Musselman, K. N., Clark, M. P., Liu, C., Ikeda, K., & Rasmussen, R. (2017). Slower snowmelt in a warmer world. *Nature Climate Change*, 7(3), 214–219. <https://doi.org/10.1038/nclimate3225>
- Neiman, P. J., Schick, L. J., Ralph, F. M., Hughes, M., & Wick, G. A. (2011). Flooding in western Washington: The connection to atmospheric rivers. *Journal of Hydrometeorology*, 12, 1337–1358.
- NEON (National Ecological Observatory Network). (2020). Total biomass map-spectrometer-mosaic (DP3.30016.001). <https://data.neonscience.org>
- Pörtner, H.-O., Roberts, D. C., Masson-Delmotte, V., Zhai, P., Tignor, M., Poloczanska, E., Mintenbeck, K., Alegria, A., Nicolai, M., Okem, A., Petzold, J., Rama, B., & Weyer, N. M. (2019). IPCC special report on The ocean and cryosphere in a changing climate.
- Raleigh, M., Livneh, B., Lapo, K., & Lundquist, J. (2016). How does availability of meteorological forcing data impact physically based snowpack simulations? *Journal of Hydrometeorology*, 17, 99–120.
- Rush, M. J., & Rajaram, H. (2022). Influence of snowpack cold content on seasonally frozen ground and its hydrologic consequences: A case study from Niwot Ridge, CO. *Water Resources Research*, 58(9), e2021WR031911.
- Stein, M. (1987). Large sample properties of simulations using Latin hypercube sampling. *Technometrics*, 29(2), 143–151.
- Sun, N., Yan, H., Wigmosta, M. S., Leung, L. R., Skaggs, R., & Hou, Z. (2019). Regional snow parameters estimation for large-domain hydrological applications in the Western United States. *Journal of Geophysical Research: Atmospheres*, 124(10), 5296–5313.
- Tang, Q., & Lettenmaier, D. P. (2012). 21st century runoff sensitivities of major global river basins. *Geophysical Research Letters*, 39(3), L06403.
- Tarboton, D. G., Bras, R. L., & Rodriguez-Iturbe, I. (1991). On the extraction of channel networks from digital elevation data. *Hydrological Processes*, 5(1), 81–100.
- Trujillo, E., & Molotch, N. P. (2014). Snowpack regimes of the western United States. *Water Resources Research*, 50, 5611–5623. <https://doi.org/10.1002/2013WR014753>

- Trujillo, E., Molotch, N. P., Goulden, M. L., Kelly, A. E., & Bales, R. (2012). Elevation-dependent influence of snow accumulation on forest greening. *Nature Geoscience*, 5(10), 705–709. <https://doi.org/10.1038/ngeo1571>
- Vionnet, V., Six, D., Auger, L., Dumont, M., Lafaysse, M., Quéno, L., Réveillet, M., Dombrowski-Etchevers, I., Thibert, E., & Vincent, C. (2019). Sub-kilometer precipitation datasets for snowpack and glacier modeling in alpine terrain. *Frontiers in Earth Science*, 7, 182.
- Viviroli, D., Dür, H. H., Messerli, B., Meybeck, M., & Weingartner, R. (2007). Mountains of the world, water towers for humanity: Typology, mapping, and global significance. *Water Resources Research*, 43, 1–13.
- Whitaker, A., Alila, Y., Beckers, J., & Toews, D. (2003). Application of the distributed hydrological soil vegetation model to Redfish Creek, British Columbia: Model evaluation using internal catchment data. *Hydrological Processes*, 17, 199–224.
- Wieder, W. R., Kennedy, D., Lehner, F., Musselman, K. N., Rodgers, K. B., Rosenbloom, N., Simpson, I. R., & Yamaguchi, R. (2022). Pervasive alterations to snow-dominated ecosystem functions under climate change. *Proceedings of the National Academy of Sciences*, 119(30), e2202393119.
- Wigmosta, M. S., Vail, L. W., & Lettenmaier, D. P. (1994). A distributed hydrology-vegetation model for complex terrain. *Water Resources*, 30(6), 1665–1679.
- Williams, M. W., Brooks, P. D., Mosier, A., & Tonnessen, K. A. (1996). Mineral nitrogen transformations in and under seasonal snow in a high-elevation catchment in the Rocky Mountains. *United States. Water Resources Research*, 32(10), 3161–3171.
- Wlostowski, A. N., Molotch, N., Anderson, S. P., Brantley, S. L., Chorover, J., Dralle, D., Dralle, D., Kumar, P., Li, L., Lohse, K. A., Mallard, J. M., McIntosh, J. C., Murphy, S. F., Parrish, E., Safeeq, M., Seyfried, M., Shi, Y., & Harman, C. (2021). Signatures of hydrologic function across the critical zone observatory network. *Water Resources Research*, 57(3), e2019WR026635.
- Winstral, A., Elder, K., & Davis, R. E. (2002). Spatial snow modeling of wind-redistributed snow using terrain-based parameters. *Journal of Hydrometeorology*, 3(5), 524–538.
- Winstral, A., & Marks, D. (2002). Simulating wind fields and snow redistribution using terrain-based parameters to model snow accumulation and melt over a semi-arid mountain catchment. *Hydrological Processes*, 16(18), 3585–3603.
- Winstral, A., Marks, D., & Gurney, R. (2013). Simulating wind-affected snow accumulations at catchment to basin scales. *Advances in Water Resources*, 55, 64–79.
- Woods, R. A. (2009). Analytical model of seasonal climate impacts on snow hydrology: Continuous snowpacks. *Advances in Water Resources*, 32(10), 1465–1481.

SUPPORTING INFORMATION

Additional supporting information can be found online in the Supporting Information section at the end of this article.

How to cite this article: Hale, K. E., Musselman, K. N., Bjarke, N. R., Livneh, B., Hinckley, E.-L. S., & Molotch, N. P. (2024). Changes in snow water storage and hydrologic partitioning in an alpine catchment in the Colorado Front Range. *Hydrological Processes*, 38(7), e15206. <https://doi.org/10.1002/hyp.15206>